Int. J. Heat Mass Transfer. Vol. 35, No. 11, pp. 2941–2952, 1992
Printed in Great Britain

0017-9310/92 $5.00+0.00

Mixed convection from multiple-layered boards with cross-streamwise periodic boundary conditions

SEO YOUNG KIM, HYUNG JIN SUNG and JAE MIN HYUN†

Department of Mechanical Engineering, Korea Advanced Institute of Science and Technology, Yusung, Taejon, 305-701, Korea

(*Received* 31 *October* 1990 *and in final form* 12 *November* 1991)

Abstract—A comprehensive analysis is made of the flow and heat transfer characteristics of mixed convection in a channel with rectangular blocks attached on one channel wall. The flow geometry models the cooling process of integrated chips of high-power densities mounted on a multi-layered printed circuit board system. Extensive numerical solutions are acquired to the governing Navier–Stokes equations under the Boussinesq-fluid assumption. The finite thickness of the board is fully accounted for; the conjugate nature of the heat transfer within a single module is described. In an effort to move closer to realism, the thermally-periodic boundary condition is imposed on the two successive plates. Details of the flow and thermal fields, for Reynolds numbers ranging from 100 to 1500 and Grashof numbers in the range of 0 to 2×10^6, are presented for two representative cases, i.e. a horizontally-oriented channel and a vertically-oriented channel. The behavior of the local Nusselt number along the block surfaces is portrayed. The distributions of the temperature and of the heat transfer rate on the surface of the base plate are illustrated. The trend of the maximum chip temperature vs *Re* is depicted. In light of the conjugate heat transfer analyses of the present study, it is asserted that such oversimplified assumptions as the isothermal or adiabatic surface wall conditions may not be entirely appropriate for simulating the cooling of modern electronic devices.

1. INTRODUCTION

ONE OF the serious requirements in the design and operation of modern high-powered electronic technologies has been an efficient thermal control of the system. For instance, the power densities in the state-of-the-art electronic computers are extremely high. Consequently, unless an effective removal of the excessive heat generated within the devices is in place, performance of these sensitive electronic devices deteriorates rapidly.

The principal elements in these sophisticated electro-mechanical systems are the arrays of chips mounted on a printed circuit board (PCB). The chips convert the electrical power input into thermal energy, and therefore the cooling of the chips is an issue of central concern [1]. The common practice is to utilize the fluid flow in one form or another; the heat transport between the PCBs and the chip blocks depends mostly on the convective heat transfer processes. Figure 1 shows a sketch of the flow and heat transfer problems in hand.

A perusal of the relevant literature reveals that this problem has been a subject of active research. For example, Ramadhyani *et al.* [2] made numerical studies of conjugate heat transfer from small isothermal heat sources embedded in a large substrate in the laminar forced convection regime. Davalath and Bayazitoglu [3] examined numerically the forced convection cooling of rectangular blocks, using the Reynolds number and the spacing between the blocks as the variable parameters. It is important to note that they treated the PCBs as either adiabatic or conducting; and the essential features of the forced convection were studied.

In response to the demands for higher-performance electronic systems, the packaging has become denser and the temperature differentials in the system have increased. This brings about a significant impact caused by the effects of natural convection. The heat transfer in the present consideration therefore constitutes a problem of mixed convection, and this forms the main topic of this paper.

The literature on the general subject of mixed convection heat transfer is extensive [4]. For instance, Pera and Gebhart [5] made experimental investigations on the interactions between laminar natural convection thermal plumes. Jaluria [6] addressed the interactions of natural convection wakes arising from thermal sources on a vertical surface. Habchi and Acharya [7] dealt with the laminar mixed convection about a symmetrically or asymmetrically heated vertical plate. Kennedy and Zebib [8] focused on the heat transfer characteristics and flow patterns resulting from four specific local heat sources. Two-dimensional mixed convection on a horizontal and a vertical adiabatic plate was investigated experimentally by Jaluria *et al.* [9, 10]. As to the mixed convection in a parallel channel, Maughan and Incropera [11] made experimental measurements in the thermal entry region for various channel inclinations. Braaten and

†To whom correspondence should be addressed.

NOMENCLATURE

B	plate thickness
C	spacing between the neighboring plates
C_p	specific heat at constant pressure
d	spanwise gap between the IC chips
F	step function which draws a line between the horizontal and the vertical cases
g	acceleration due to gravity
G	step function which is zero everywhere, except at the mid-height of the block
Gr	modified Grashof number ($g\beta qL^3/4kv^2$)
H	height of block
H_1	height of heat sources from the plate surface on which IC chips are mounted
k	thermal conductivity
L	length of block
L_1	upstream length from the first block
L_2	downstream length from the last block
L_t	total length of the plate
Nu	local Nusselt number
P	dimensionless pressure ($P = p/\rho U_0^2$)
Pe	Peclet number ($Pe = RePr = U_0L/\alpha$)
Pr	Prandtl number (v/α)
q	heat per unit length
$\dot{q}$	heat per unit volume ($\dot{q} = q/WL$)
Q'	dimensionless heat input ($Q' = 4\dot{q}L^2/q = 4L/W$)
Re	Reynolds number (U_0L/v)
S	spacing between the blocks
T_0	uniform inlet temperature
T	temperature
U_0	uniform inlet velocity
u, v	dimensionless velocity components
U, V	dimensionless velocity components ($U = u/U_0$, $V = v/U_0$)
W	width of the heat source
x, y	physical coordinates
X, Y	dimensionless x, y coordinates ($X = x/L$, $Y = y/L$).

Greek symbols

α	thermal diffusivity
β	coefficient of volumetric expansion
Θ	dimensionless temperature ($(T-T_0)/(q/4k)$)
v	kinematic viscosity of fluid
ρ	density of fluid
Ψ	dimensionless stream function.

Subscripts

0	reference value
max	maximum
s	solid region
w	wall.

Patankar [12] carried out numerical computations for three-dimensional situations under similar flow conditions. These publications have presented detailed information on the principal characteristics of mixed convection about a plate or inside a channel.

For the flow geometry in the present study, major considerations should be given to the fact that one or several blocks are attached to an inside wall surface of the channel. Therefore, a proper modeling of the interactive nature surrounding these blocks and the bounding PCB plates is of paramount importance. As illustrated schematically in Fig. 2, the thermal performance of the whole system depends crucially on the removal by the fluid stream of the heat generated by the chip blocks. The earlier papers by Patankar *et al.* [13–15] and Knight and Crawford [16] delineated the heat transfer characteristics of the flow configuration in a similar manner to that in Fig. 2. However, these works were concerned with the situations in which there exist a large number of blocks mounted on very long PCBs. These authors portrayed the flow with streamwise periodicity between the successive blocks/fins by invoking the assumption of a fully developed flow. Limitations of these models may be found in the cases when the streamwise length of PCBs is finite such that the flows at the exit may not be taken to be fully developed. Also, if the number of blocks is small, the streamwise periodicity between

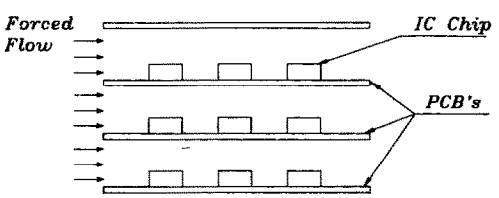

FIG. 1. Schematic of flow configuration.

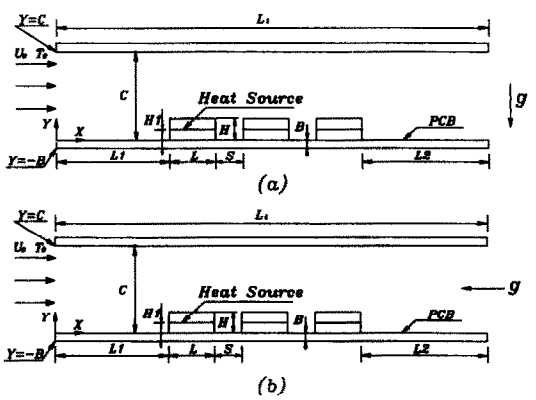

FIG. 2. Flow geometries. (a) Horizontal channel. (b) Vertical channel.

the blocks may not be fully attainable. These flow conditions are of prime relevance to certain practical high-performance electronic devices. It is proposed in this paper to examine the properties of mixed convection prevailing over the flow configurations described above. One of the key ingredients in the modeling of these flow fields is in the treatment of the thermal conditions applicable on the PCB plates, as shown in Fig. 2. The majority of past endeavors has taken the plates to be either isothermal or adiabatic [7, 10, 17]. The specification of such thermal conditions greatly simplifies the analyses; however, no in-depth evaluations of the appropriateness of such treatments have been reported in the literature. It is emphasized that a PCB plate is of finite thickness and, consequently, it has finite thermal conductivity; the conductive heat transport from the chips to the PCBs can hardly be neglected, especially for devices of high power-density. These considerations point to the inadequacy of such simplistic thermal boundary conditions as isothermal or adiabatic PCBs. The impetus of the present paper is placed on exploring more realistic and physically meaningful thermal considerations on the PCBs; these efforts will lead to an improved understanding of the complicated flow and heat transfer characteristics that take place in the cooling processes of high-density electronic packagings.

Davalath and Bayazitoglu [3] noted the significance of the thermal interactions between the fluids in the channel and the thermally-conducting neighboring PCB plates. In the present study, we shall take, as a single module, the flow domain in the cross-stream direction, $-B \leqslant Y \leqslant C$. It should be pointed out that, by this treatment, the finite thickness of a PCB is duly accounted for. Also, it is important to require that, as far as a single module is concerned, the conditions at $Y = -B$ should be identical to those at $Y = C$. In practice, these indicate periodicity of the boundary conditions in the cross-stream direction. We shall seek numerical solutions to the governing Navier–Stokes equations for the afore-mentioned single module in its entirety. Therefore, the conjugate heat transfers in the blocks and the PCBs are fully accommodated in the numerical analyses. In realistic electronic packagings, there are a large number of parallel PCBs; consequently, for the cooling of a multitude of PCB layers, the afore-mentioned periodic nature of flow conditions in the cross-stream direction appears to be a powerful and useful argument. In the present study, we shall adopt this line of reasoning; the mixed convective heat transports in such a canonical flow configuration in a multi-layered PCB system will be examined.

2. THE MATHEMATICAL MODEL AND NUMERICAL METHODS

In order to formulate a mathematically tractable problem, we consider a single module of two-dimensional steady laminar flow passing inside a parallel channel, as illustrated in Fig. 2. For practical situations in electronic packaging, the ratio of the block height H to the channel width C is in the range $H/C = 0.3$–0.4. It should be mentioned that the present flow geometry closely resembles realistic electronic packagings in common use. In the present work, we shall consider the orientation of PCBs to be either horizontal (shown in Fig. 2(a)) or vertical (Fig. 2(b)); as observed by Habchi and Acharya [7], the overall heat transfer properties are sensitive to the inclination of the main stream with respect to the gravity. Our task is to describe the flow and the associated heat transfer characteristics inside the channel. In the present treatment, all the physical properties of the fluid are taken to be constant.

The governing equations are the well-known Navier–Stokes equations. Under the Boussinesq-fluid approximation, these equations, expressed in properly nondimensionalized form, are

$$\frac{\partial U}{\partial X} + \frac{\partial V}{\partial Y} = 0 \tag{1}$$

$$U\frac{\partial U}{\partial X} + V\frac{\partial U}{\partial Y} = \frac{\nu^*}{Re}\left(\frac{\partial^2 U}{\partial X^2} + \frac{\partial^2 U}{\partial Y^2}\right) - \frac{\partial P}{\partial X} + \frac{Gr}{Re^2}\cdot\Theta\cdot F \tag{2}$$

$$U\frac{\partial V}{\partial X} + V\frac{\partial V}{\partial Y} = \frac{\nu^*}{Re}\left(\frac{\partial^2 V}{\partial X^2} + \frac{\partial^2 V}{\partial Y^2}\right) - \frac{\partial P}{\partial Y} + \frac{Gr}{Re^2}\cdot\Theta\cdot[1-F] \tag{3}$$

$$U\frac{\partial \Theta}{\partial X} + V\frac{\partial \Theta}{\partial Y} = \frac{k^*}{Pe\cdot c^*}\left(\frac{\partial^2 \Theta}{\partial X^2} + \frac{\partial^2 \Theta}{\partial Y^2}\right) + \frac{Q'}{Re\cdot Pr}\cdot G. \tag{4}$$

In the above, nondimensionalizations were executed by adopting L, U_0 (the incoming flow velocity), and ρU_0^2 for the scale lengths, velocity, and pressure, respectively. In equations (2)–(4), the gravitational buoyancy appears in the last term. Accordingly, the index $F = 0.0$ for the configuration of Fig. 2(a) is conveniently termed as the horizontal channel; $F = 1.0$ for the configuration of Fig. 2(b), illustrating the vertical channel. The generation of heat from the chip block is modeled by the last term in equation (4); G is a step function which is zero everywhere except at the mid-height of the block $Y = H_1$, where $G = 1.0$. In the above, the major nondimensional parameters are defined as

$$Re \text{ (Reynolds number)} \equiv U_0 L/\nu \tag{5}$$

$$Gr \text{ (Grashof number)} \equiv g\beta q L^3/(4k\nu^2) \tag{6}$$

$$Pr \text{ (Prandtl number)} \equiv \nu/\alpha \tag{7}$$

$$Pe \text{ (Peclet number)} \equiv Re\cdot Pr = U_0 L/\alpha \tag{8}$$

where q is the heat generation per unit length. Also, we note that the ratio of thermal conductivity of the solid material, k_s, to that of the fluid, k, is denoted by $k^*(\equiv k_s/k)$; similarly, $\nu^*(\equiv \nu_s/\nu)$ and $c^*[\equiv(\rho C_p)_s/(\rho C_p)]$ designate respectively the ratios of viscosities and thermal capacities of the solid and the fluid. In equations (2)–(4), in the regions occupied by the fluid, ν^*, k^*, and c^* are unity. Only in the domains occupied by the solid parts should proper values of ν^*, k^*, and c^* be used (see below).

As shown in Figs. 1 and 2, the block is of width L and height H; the cartesian coordinates (X, Y), with the corresponding velocity components (U, V), are indicated therein. In the present study, we shall specifically consider the geometrical configuration in which three blocks are contained. These three-block systems are reasonably simple so that detailed computational analyses are possible; at the same time, the three-block configurations possess most of the essential features that are peculiar to the channel flow in which a multitude of blocks are located. Accordingly, the present study of the three-block channel flow model represents a compromise between a computationally feasible problem and a reasonably realistic practical problem formulation.

The associated boundary conditions for the velocity field are:

for $0 < X < L_t$,

$$\text{at } Y = 0, \quad U = V = 0 \tag{9}$$

$$\text{at } Y = C, \quad U = V = 0 \tag{10}$$

$$\text{at } Y = -B, \quad U = V = 0; \tag{11}$$

for $0 < Y < C$,

$$\text{at } X = 0, \quad U = 1, \quad V = 0; \tag{12}$$

for $-B < Y < C$,

$$\text{at } X = L_t, \quad \frac{\partial U}{\partial X} = \frac{\partial V}{\partial X} = 0. \tag{13}$$

For the temperature field, the boundary conditions are:

$$\text{for } 0 < Y < C, \quad \text{at } X = 0, \quad \Theta = 0 \tag{14}$$

$$\text{for } -B < Y < 0, \quad \text{at } X = 0, \quad \frac{\partial \Theta}{\partial X} = 0 \tag{15}$$

$$\text{for } -B < Y < C, \quad \text{at } X = L_t, \quad \frac{\partial \Theta}{\partial X} = 0 \tag{16}$$

$$\text{for } 0 < X < L_t, \quad \Theta(X, C) = \Theta(X, -B),$$

$$\frac{\partial \Theta}{\partial Y}(X, C) = \frac{\partial \Theta}{\partial Y}(X, -B). \tag{17}$$

As stressed previously, the entire flow domain, $-B \leqslant Y \leqslant C$, $0 \leqslant X \leqslant L_t$ is treated for analysis. For the regions occupied by the solid parts, i.e. the finite thickness of the base plate and the blocks, the appropriately selected values (k_s, ν_s, C_{ps}) will be assigned. This is an effective way to deal with the conjugate nature of the convection–conduction between the flowing fluid and the solid parts.

Some comments are in order for the modeling of the IC chips. In the present work, an IC chip is idealized as a rectangular block of length L and height H. This reflects an effort to produce a realistic model; in actual situations, the silicon chip, which generates heat, is surrounded by a plastic mould compound. This is modeled in the present study as a rectangular block with the heat generating part embedded at the mid-height of the block.

Equations (9)–(13) refer to the usual no-slip conditions on all the solid walls, and the assumptions of a uniform flow at the inlet and the fully developed conditions at the outlet of the channel. The crux of the present model lies in the cross-streamwise periodic boundary conditions across a single module of the multi-layer channel system, and this is reflected in equation (17). Consequently, the periodicity is applicable to the temperature as well as the temperature gradients at $Y = C$ and $Y = -B$. As ascertained earlier, the finite thickness of the base plate is fully accounted for.

In order to solve the above system of equations, the well established numerical solution scheme based on the SIMPLER algorithm of Patankar [18] was utilized. In the actual computations, for the regions occupied by the solid parts, $\nu^*(\equiv \nu_s/\nu) = 10^{10}$, $k^*(\equiv k_s/k) = 10$, and $c^*[\equiv(\rho C_p)_s/(\rho C_p)] = 1.0$ were used [3]. Obviously, the concept of kinematic viscosity for solid parts is introduced merely to facilitate convenience of numerical computations. Clearly, by setting $\nu^* = 10^{10}$ for the solid portions, the corresponding velocities would be effectively zero $(U, V \sim 10^{-25})$. By resorting to this method, the diffusion term in the energy equation can handle both the fluid and solid regions as one calculation domain, with zero velocities in the solid regions. For numerical computations of the energy equation, the resulting finite difference algebraic equation was solved by using CTDMA (Cyclic TriDiagonal Matrix Algorithm), which was well documented by Patankar *et al.* [13]. This methodology represents a special case of the Gaussian elimination procedure, and it has been found to be adequate to deal with the thermally periodic nature in the Y-direction. No specifications of the wall temperatures are required in this formulation; in the actual calculations, underrelaxation had to be introduced to achieve converged solutions of the temperature field.

All the computations were performed on a 101×41 grid network. In the X-direction, the grid points were crowded near the blocks; in the Y-direction, the grid points were clustered near the top and bottom surfaces of the channel as well as in the vicinity of the blocks. Approximately 7000 iterations were needed to obtain the pre-assigned convergence in the velocity and temperature fields. The computations were implemented on a Cray 2-S supercomputer, and a typical computer

CPU time was approximately 50 min for one set of calculations. In the present study, convergence was declared when the maximum changes in dimensionless values of U, V and Θ between two successive iterations were less than 10^{-4}. Several trial calculations were repeated to monitor the sensitivity of the results to the grid size, and the outcome of these tests was satisfactory.

With the converged solutions in hand, extensive post-processings of the numerical data were conducted. As usual, a physical quantity of great interest is the local Nusselt number, Nu, along the surfaces of the solid walls. The definition of Nu has been given as

$$Nu = -\frac{1}{\Theta_w}\cdot\frac{\partial\Theta}{\partial n} \tag{18}$$

where n denotes the direction normal to the solid surface.

3. RESULTS AND DISCUSSION

The geometrical particulars of the present calculations were set forth: $L = 1.0$, $L_1 = 4.0$, $L_2 = 21.0$, $H = 0.35$, $H_1 = 0.135$, $B = 0.15$, $C = 1.05$, $S = 1.0$, $W = 0.04$. These values are representative of the shapes of frequent occurrence in fluid cooling of the high-tech electronic devices in industrial use [3]. It is noted that, with the above values of L_1 and L_2, the uniformity of the entrance flow conditions as well as the continuity in the exit flow (equations (12) and (13)) is satisfied to a fair degree of accuracy (see ref. [7]).

3.1. *Horizontal channel*

Initially, we shall examine the cases of a horizontal channel, as portrayed in Fig. 2(a). Figure 3 illustrates the effects of buoyancy on the global flow structure. A series of calculations was carried out by varying the strength of the mixed convection, Gr/Re^2, in the range of 0–50, while the Reynolds number was fixed at $Re = 100$. Scrutiny of the numerical results discloses several interesting features. When Gr/Re^2 is very small, say less than $O(1)$, the streamline patterns are rather insensitive to the variation in Gr/Re^2. The flow fields displayed in Figs. 3(a)–(c) reveal the complex nature of the flow behavior for a multi-block system inside a channel [3, 17]. However, as Gr/Re^2 increases (see Fig. 3(d)), the buoyancy effects become eminent; the reattachment point downstream of the last block is delayed further downstream. Alternatively, owing to the significant influence of the buoyancy, the overall size of the recirculating zone after the last block increases. This can be explained by noting that the strong buoyancy effect causes the streamlines to be uplifted from the surfaces of the blocks. Consequently, the dividing streamline, which separates the recirculating zone, has to travel a longer distance in comparison to the case of a purely forced convective flow.

Figure 4 exhibits the flow fields under a fixed value of $Gr\,(\equiv 5\times 10^5)$, while Re is allowed to vary. The recirculating zone after the last block increases in size as Re increases. This is a well documented phenomenon; as the effect of forced convection strengthens, the recirculating zone widens and the overall flow intensifies. The results of Figs. 3 and 4 are not unexpected and the present numerical solutions provide confirmation to these flow processes. It is notable in Fig. 3(d) that, when the effects of natural convection are substantial, there appear small, weak eddies in addition to the primary eddies in the gaps between the blocks. These additional eddies rotate in the direction opposite to that of the primary eddies between the blocks. This is also attributable to the workings of the buoyancy effects; the fluid rises upward in the vicinity of the block surface under substantial buoyancy effects. This generates small and weak counter-rotating eddies near the forward face of the rearward-located block.

Figure 5 displays the temperature fields for varying Reynolds numbers, while the Grashof number is fixed at $Gr = 5\times 10^5$ and $Pr = 0.7$. As is evident in Fig. 5(a), when the Peclet number ($Pe \equiv Re\cdot Pr$) is small,

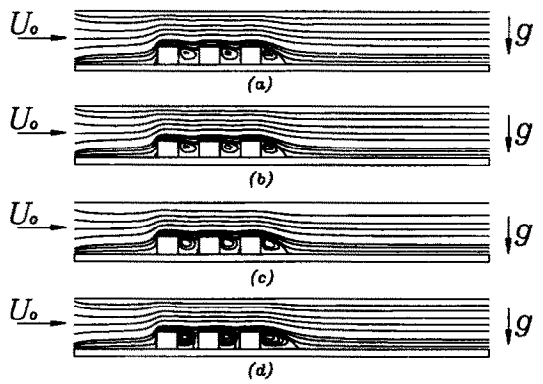

FIG. 3. Stream patterns for the horizontal channel. $Pr = 0.7$, $Re = 100$; the contour values are $\Psi = -0.02$, -0.01, 0, 0.01, 0.05, 0.1, and beyond $\Psi = 0.1$, the interval $\Delta\Psi = 0.2$. (a) $Gr/Re^2 = 0$, $-\Psi_{max} = 0.023$; (b) $Gr/Re^2 = 1$, $-\Psi_{max} = 0.024$; (c) $Gr/Re^2 = 10$, $-\Psi_{max} = 0.028$; (d) $Gr/Re^2 = 50$, $-\Psi_{max} = 0.045$.

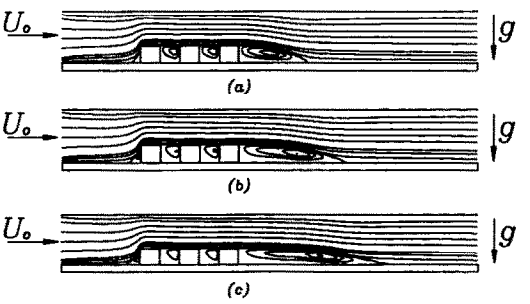

FIG. 4. Stream patterns for the horizontal channel. $Pr = 0.7$, $Gr = 5\times 10^5$. (a) $Re = 500$, $Gr/Re^2 = 2$, $-\Psi_{max} = 0.035$; (b) $Re = 1000$, $Gr/Re^2 = 0.5$, $-\Psi_{max} = 0.040$; (c) $Re = 1500$, $Gr/Re^2 = 0.22$, $-\Psi_{max} = 0.042$.

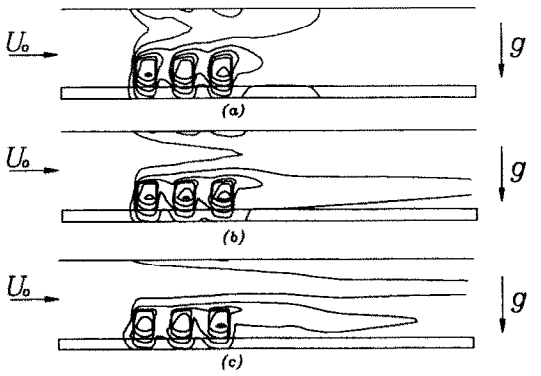

FIG. 5. Isotherm contours for the horizontal channel. $Pr = 0.7$, $Gr = 5 \times 10^5$; the contour values are $\Theta = 0.001$, 0.01, beyond $\Theta = 0.01$, the interval $\Delta\Theta = 0.02$. (a) $Re = 100$, $Gr/Re^2 = 50$, $\Theta_{max} = 0.137$; (b) $Re = 500$, $Gr/Re^2 = 2.0$, $\Theta_{max} = 0.107$; (c) $Re = 1500$, $Gr/Re^2 = 0.22$, $\Theta_{max} = 0.094$.

the regions where the effects of the blocks are felt tend to be localized to the neighborhood of the blocks (see Figs. 5(a) and (b)). However, at large Peclet numbers, distinct thermal boundary layers at the top and bottom surfaces of the channel are in evidence. At a still higher Peclet number (see Fig. 5(c)), the thermal boundary layers at the top and bottom surfaces of the channel are thinner, and they do not meet each other until the exit of the channel. These findings are in qualitative agreement with the earlier observations of Davalath and Bayazitoglu [3]. Therefore, when the Peclet number is very high, the present results, which are based on the conjugate heat transfer analysis using the cross-streamwise periodic boundary conditions (equation (17)), suggest that the top and bottom surfaces of the channel are not in direct thermal communication.

Figure 6 exemplifies the behavior of the local Nusselt number along the block surfaces for a fixed Reynolds number ($Re = 100$). For a given block, the maximum heat transfer takes place at the front corner. In these regions, the curvature of the streamline becomes very large locally, and the accompanying local Nusselt number is large. It is also remarked that, as the fluid passes over the blocks, the temperature of the fluid increases. Consequently, the temperature

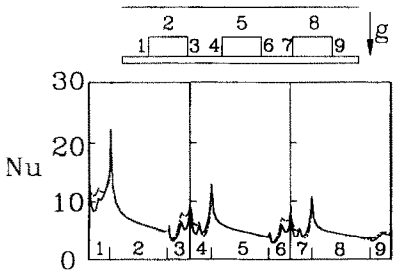

FIG. 6. Local Nusselt number variation along the block surface for the horizontal channel. $Pr = 0.7$, $Re = 100$. (———) $Gr = 0.0$, $Gr/Re^2 = 0.0$; (– – –) $Gr = 10^4$, $Gr/Re^2 = 1.0$; (— · —) $Gr = 5 \times 10^5$, $Gr/Re^2 = 50$.

difference between the fluid and the block decreases as the fluid moves downstream; as a result, the local Nusselt number decreases progressively for the second and third blocks. As anticipated, the local Nusselt number increases as the effect of the buoyancy strengthens. However, it should be pointed out that the influence of mixed convection is prominent, principally near the vertical faces of the block. On the bulk of the horizontal surface of the block, the local Nusselt number remains virtually unchanged as Gr/Re^2 varies. Over much of the forward part of the horizontal surface of a block, the buoyancy-generated flow is swept away by the forced flow; therefore, for the parameter ranges adopted in the present study, the impact of mixed convection is confined to over the vertical faces.

As stressed earlier, a main purpose of this paper is to investigate the heat transfer characteristics by specifying more realistic thermal conditions at the plates. It is therefore useful to appraise the differences in the results between those obtained by using the present thermal conditions and the other conventional treatments. Figure 7 exhibits the computed results showing the temperature along the bottom surface of the base plate, i.e. at $Y = -B$. (Note that, due to the cross-streamwise periodicity imposed in the present analysis, these results also refer to the conditions along the top surface of the channel, i.e. $Y = C$.) The temperature plots in Fig. 7(a) demonstrate substantial variations near the areas where the blocks are located. Downstream of the last block, the wall temperature

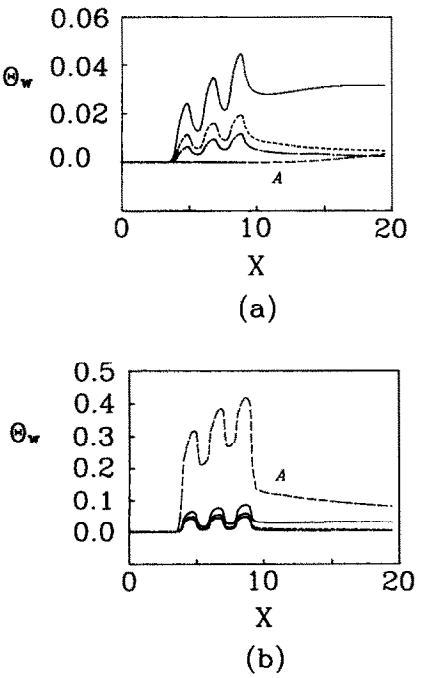

FIG. 7. Surface temperature profiles. $Pr = 0.7$, $Gr = 5 \times 10^5$. (a) Along the bottom surface of the base plate (along $Y = C$). (b) Along the top surface ($Y = 0$). (———) $Re = 100$; (– – –) $Re = 500$; (— · —) $Re = 1500$. Curves A refer to the results obtained for the adiabatic base plate at $Re = 500$.

does not vary much until the fluid passes out through the exit. The efficiency of cooling, measured in terms of the reduction of the wall surface temperature, is noticeable as the influence of the forced convection strengthens, i.e. Re increases. For comparison purposes, parallel computations were performed for the same geometry by using the assumption that the base plate was thermally insulated. For the case of adiabatic plates, it is illustrated in Fig. 7(a) that the wall temperature along the bottom surface of the plate, at $Y = C$, remains substantially unchanged as the fluid travels downstream. Figure 7(b) displays the temperature profiles along the top surface of the base plate, i.e. at $Y = 0$. The blocks are attached to this surface; therefore, the temperature along this surface is appreciably higher than that along $Y = C$. (Note the difference in scales of the ordinates of Figs. 7(a) and (b).) When the base plate is adiabatic, the fluid in the vicinity of this surface, at $Y = 0$, has to carry away all the thermal energy generated in the blocks, since no heat transfer across the base plate is allowed. Consequently, if the base plate is assumed to be adiabatic, the temperature at this surface ($Y = 0$) is much higher than for the case of more realistic thermal conditions. In summary, the observations of Fig. 7 point to an important conclusion as to the inadequacy of such customary assumption as the adiabatic base plate, which was invoked in some preceding work (e.g. refs. [3, 17]).

Figure 8 displays the comparisons between the present results and the solutions obtainable under the assumption of isothermal base plates. Figure 8(a) shows the Nusselt number profiles along the bottom surface of the plate, i.e. $Y = C$. Evidently, heat transfer from the plate to the fluid is intense in the regions where the blocks are located, and this trend is pronounced as Re increases. The plots in Fig. 8(b) illustrate Nu along the surface $Y = 0$. In the present model of conjugate heat transfer analysis, in the regions where the blocks are located, the heat generated at the mid-height inside the block (at $Y = H_1$) is transported to the base plate by conduction. Therefore, in the plots of Fig. 8(b), the Nusselt number at the surface $Y = 0$, excluding the portions occupied by the blocks (namely $A \leqslant X \leqslant B, C \leqslant X \leqslant D, E \leqslant X \leqslant F$), is illustrated. For these portions, the conductive heat transfer, shown by $\partial\Theta/\partial Y|_{Y=0}$ in the solid, is depicted in Fig. 8(c). For comparison purposes, the results of the parallel calculations, made under the assumption of the isothermal base plate, are shown in Fig. 8. As anticipated, the temperature profiles thus obtained bear general similarity to the results of an ordinary channel flow with isothermal wall surface conditions [11]. The findings demonstrated in Fig. 8 also suggest the inadequacy of the usual assumption of the isothermal surface conditions in dealing with the complex heat transfer properties in these realistic systems. As portrayed by the present analyses, the heat transfers in the regions of the blocks are eminent; the predictions of the prior work (e.g. ref. [7]), which invoked the condition of isothermal base plates, tend to underestimate the actual heat transfer rates.

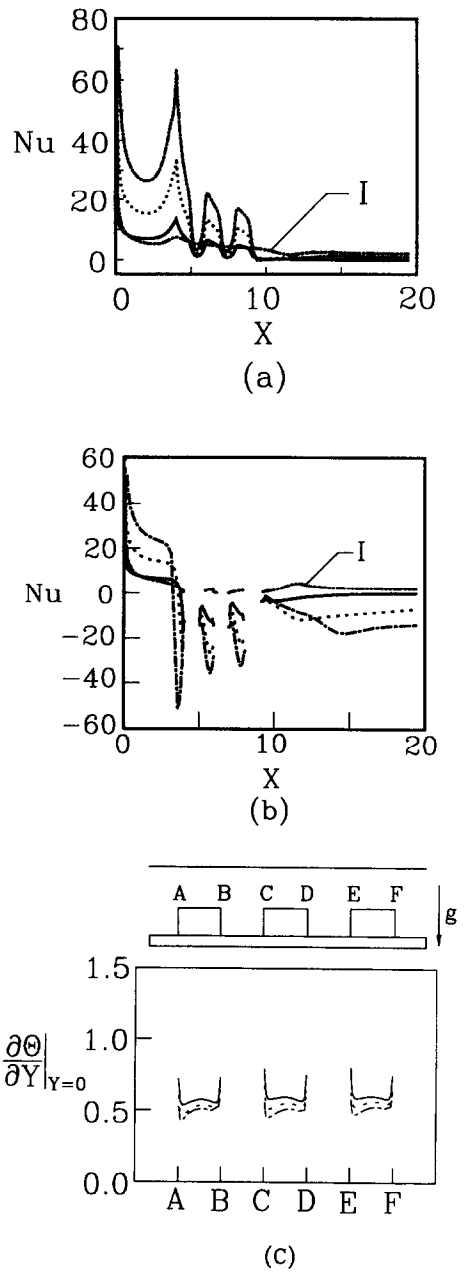

FIG. 8. Nusselt number profiles. $Pr = 0.7$, $Gr = 5 \times 10^5$. (a) Along the bottom surface of the base plate (along $Y = C$). (b) Along the top surface $Y = 0$, excluding the portions occupied by the blocks. (c) Conductive heat transport at $Y = 0$ in the portions occupied by the blocks. (———) $Re = 100$; (– – –) $Re = 500$; (— · —) $Re = 1500$. Curves I refer to the results obtained for the isothermal base plate at $Re = 500$.

3.2. *Vertical channel*

Now, we shall summarize in Figs. 9–15 the results pertaining to the vertically-oriented channel, a flow configuration depicted in Fig. 2(b). As shown in Fig.

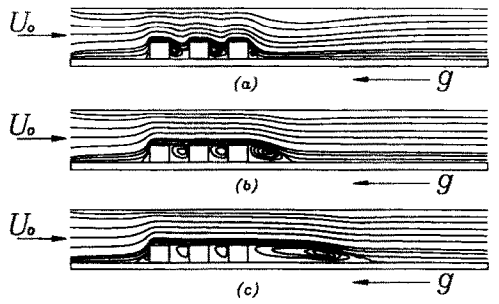

FIG. 9. Stream patterns for the vertical channel (assisting case). $Pr = 0.7$, $Gr = 5 \times 10^5$. (a) $Re = 100$, $Gr/Re^2 = 50$, $-\Psi_{max} = 0.050$; (b) $Re = 500$, $Gr/Re^2 = 2$, $-\Psi_{max} = 0.045$; (c) $Re = 1500$, $Gr/Re^2 = 0.22$, $-\Psi_{max} = 0.046$.

9, for a fixed value of Gr, the recirculating zone behind the last block increases in size as Re increases, a result which is in qualitative accord with the preceding observation shown in Fig. 4. The plot in Fig. 9(a) is similar to a purely buoyancy-driven flow about a vertically-oriented, multi-block system (see ref. [19]). The impact of the forced convection is minor (Gr/Re^2 large), and the overall flow field demonstrates the characteristics revealed by the buoyant flows in the wakes of upstream blocks (see ref. [7]).

The temperature fields are displayed in Fig. 10 for a fixed Gr ($=5 \times 10^5$) and Pr ($=0.7$). As asserted previously for a horizontal channel (see Fig. 5), when the Peclet number is small (see Fig. 10(a)), the global temperature fields are strongly interrelated, encompassing the entire domain from the bottom to the top surfaces of the channel. However, for a high Peclet number (see Fig. 10(c)), the formation of distinct thermal boundary layers near both the top and bottom surfaces of the channel is clearly seen. These findings are qualitatively similar to those of a horizontal channel.

The distribution of the local Nusselt number obtained at a fixed value of $Re = 100$, $Pr = 0.7$, along the block surfaces is shown in Fig. 11. Again, the maximum heat transfer occurs near the front corner of each block. A notable feature now is the appreciable variation of the Nusselt number with Gr along the top surfaces, i.e. surfaces 2, 5 and 8 in Fig. 11, of the blocks; this is in contrast to the case of a horizontal channel (compare Fig. 11 with Fig. 6). In the case of a vertical channel, the forced flow from the inlet and the buoyancy-driven flow are augmenting each other. Consequently, a change in the buoyancy effect causes a substantial influence on the local heat transfer rate from the surfaces that are parallel to the base plate. The plots in Fig. 11 clearly demonstrate the mutually-cooperative nature of the mixed convection for this type of flow geometry. The numerical results presented in Fig. 11 provide an example to emphasize the sensitivity of the cooling efficiency to the orientation and configuration of the cooling device.

In a manner similar to Figs. 7 and 8, comparisons are presented in Figs. 12 and 13 between the present results and the results obtained by using the simplistic conditions. The trends observable in Figs. 12 and 13 are akin to those found in Figs. 7 and 8. However, for a vertically-oriented channel, the wall surface temperature is lower and the heat transfer rate is higher than for the case of a horizontal channel. As emphasized earlier, the mixed convection is cooperating for the vertical channel in the present consideration. Inspection of Figs. 12 and 13 underscores the inappropriateness of such simplistic treatments as the isothermal or adiabatic base plates. Such simplified assumptions may be useful in the regions far downstream of the last block. However, in practical technological applications, the downstream length of the base plate is finite. The results in Figs. 12 and 13 imply that the prior estimates of heat transfer [7], based on such rather oversimplified treatments of the base plate boundary conditions, may lead to misleading descriptions of the realistic systems.

In view of practical applications, the maximum temperature that is attainable in a block is a significant design parameter for high-powered electronic devices. Table 1 exemplifies this maximum temperature vs Re for air and water, for both horizontal and vertical channels. It is immediately clear from Table 1 that the

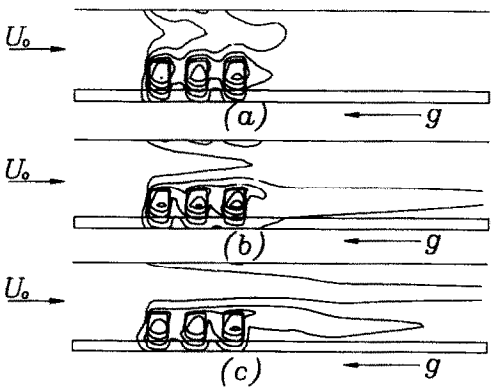

FIG. 10. Isotherm contours for the vertical channel. $Pr = 0.7$, $Gr = 5 \times 10^5$. (a) $Re = 100$, $Gr/Re^2 = 50$, $\Theta_{max} = 0.135$; (b) $Re = 500$, $Gr/Re^2 = 2$, $\Theta_{max} = 0.106$; (c) $Re = 1500$, $Gr/Re^2 = 0.22$, $\Theta_{max} = 0.093$.

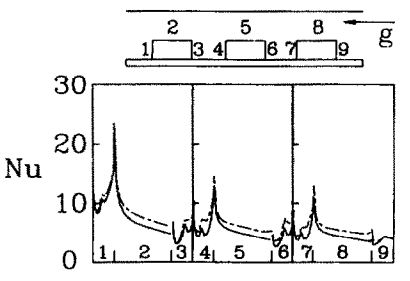

FIG. 11. Local Nusselt number variation along the block surface for the vertical channel. $Pr = 0.7$, $Re = 100$. (———) $Gr = 0$, $Gr/Re^2 = 0$; (– – –) $Gr = 10^4$, $Gr/Re^2 = 1$; (— · —) $Gr = 5 \times 10^5$, $Gr/Re^2 = 50$.

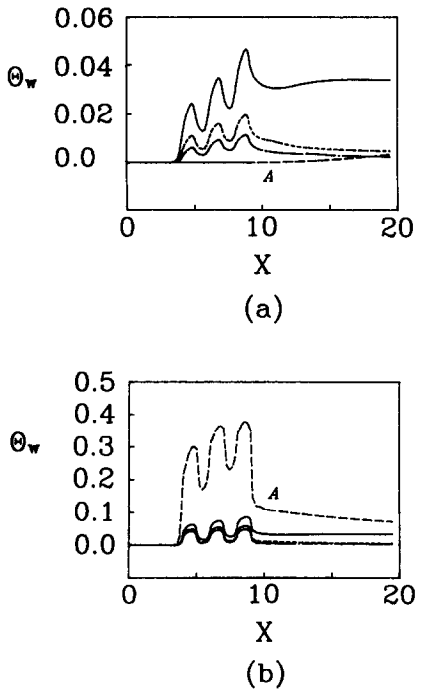

FIG. 12. Surface temperature profiles. $Pr = 0.7$, $Gr = 5 \times 10^5$. (a) Along the surface of the base plate (along $Y = C$). (b) Along the surface ($Y = 0$). (———) $Re = 100$; (– – –) $Re = 500$; (—·—) $Re = 1500$. Curves A refer to the results obtained for the adiabatic base plate at $Re = 500$.

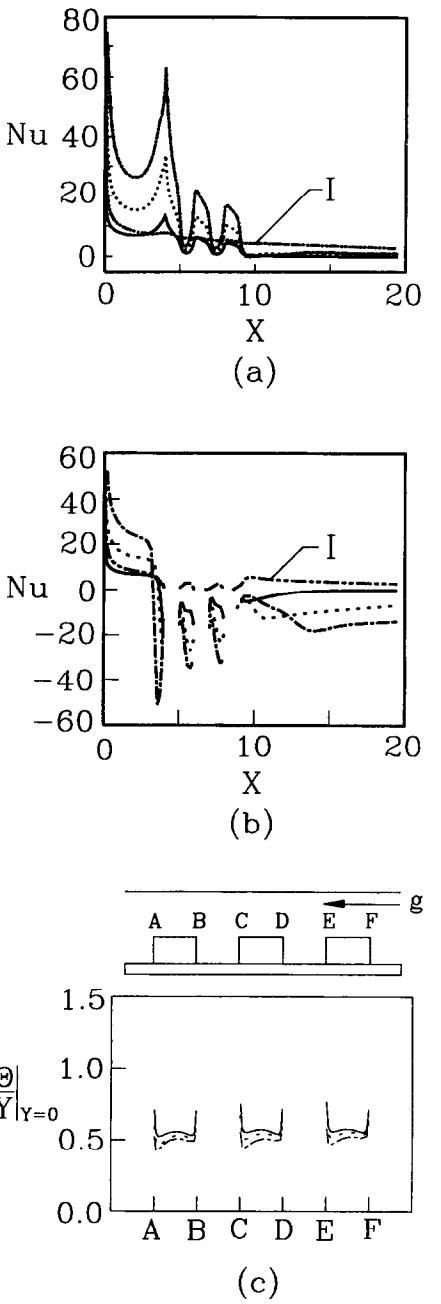

FIG. 13. Nusselt number profiles. $Pr = 0.7$, $Gr = 5 \times 10^5$. (a) Along the surface of the base plate (along $Y = C$). (b) Along the surface $Y = 0$, excluding the portions occupied by the blocks. (c) Conductive heat transport at $Y = 0$ in the portions occupied by the blocks. (———) $Re = 100$; (– – –) $Re = 500$; (—·—) $Re = 1500$. Curves I refer to the results obtained for the isothermal base plate at $Re = 500$.

maximum block temperature becomes lower as Re and Pr increase, i.e. for higher Peclet numbers. However, Table 1 discloses that the gain (in terms of the reduction of the maximum block temperature) levels off quickly as Re increases over around $Re = 900.0$. This is in accord with the previous assertion [3]. Perusal of Table 1(a) and (b) indicates that the vertically-oriented channel is slightly more effective than the horizontally-oriented channel. This can be easily understood by noting that the buoyancy-driven flow essentially aids the forced convective flow in the case of a vertical channel.

In an effort to amplify the foregoing statement, the flow and the thermal fields of the present results and the results obtainable under the adiabatic wall conditions are exemplified in Figs. 14 and 15. Substantial discrepancies are discernible between these numerically-generated plots. It is noticed that there exists an additional eddy downstream of the last block for the case of an adiabatic wall (see Fig. 14(a)). However, in the case in which the cross-streamwise periodicity is enforced, due to the finite heat flux from the base plate (see Fig. 13), such a conspicuous downstream eddy is not seen (see Fig. 14(b)). Figure 15 shows that the maximum temperature in the last block is considerably higher for the case of an adiabatic surface condition than that under the cross-streamwise periodic condition. This also suggests that, if an adiabatic base plate condition is adopted, the block temperatures are substantially overestimated.

The effect of the channel orientation is exemplified in Fig. 16. For this particular geometry, the enhancement of heat transfer by the gravity effect is discernible for the case of a vertical channel.

As illustrated above, the present numerical studies provide rather convincing evidence for the assertion that more sophisticated boundary treatments (than the customary isothermal or adiabatic plate surface

Table 1. The maximum block temperature; conditions are $Gr = 5 \times 10^5$; (a) $Pr = 0.7$, (b) $Pr = 7.0$

Re	Horizontal channel Θ_{max}	Vertical channel Θ_{max}
(a)		
100	0.137	0.135
500	0.107	0.106
1000	0.098	0.098
1500	0.094	0.093
(b)		
100	0.102	0.098
500	0.085	0.082
1000	0.079	0.078
1500	0.075	0.074

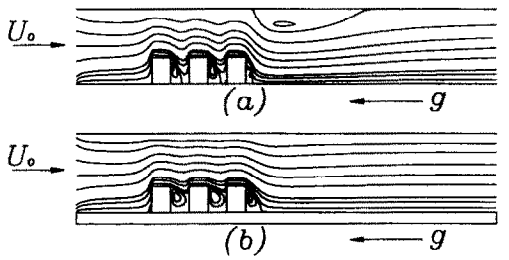

FIG. 14. Exemplary comparisons of the stream patterns. $Re = 100$, $Gr/Re^2 = 10.0$, $Pr = 0.7$. Results obtained under the assumptions of: (a) the adiabatic base plate, $-\Psi_{max} = 0.031$; (b) the cross-streamwise periodic boundary conditions, $-\Psi_{max} = 0.030$.

conditions) are called for to delineate the subtle nature of these complex systems. It is believed that the cross-streamwise periodic conditions will be more readily applicable when the overall channel height, C, decreases and/or the power density increases further. For modern micro-electronic devices, miniaturization is pursued; the thermal boundary conditions adopted in the present paper will have more relevance for these practical situations.

4. CONCLUSIONS

Far-ranging numerical simulations have been presented to capture the essentials of mixed convective heat transfer inside a channel. The conjugate nature

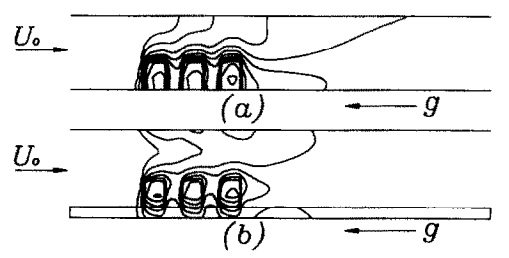

FIG. 15. Exemplary comparisons of the isotherm contours. $Re = 100$, $Gr/Re^2 = 10.0$. (a) The adiabatic base plate, $\Theta_{max} = 0.448$. (b) The cross-streamwise periodic boundary conditions, $\Theta_{max} = 0.137$.

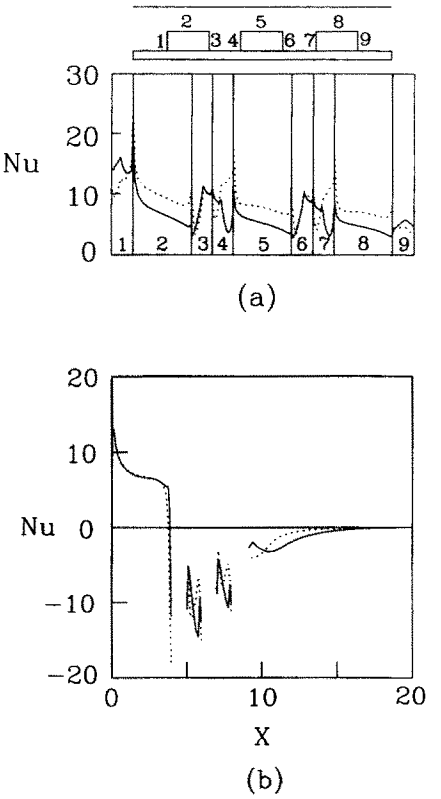

FIG. 16. Exemplary comparisons of the local Nusselt numbers between a horizontal channel (———) and a vertical channel (– – –). Conditions are $Gr/Re^2 = 200.0$ and $Gr = 2 \times 10^6$. (a) Along the block surface. (b) Along the surface ($Y = 0$), excluding the portions occupied by the blocks.

of heat transfer is fully accommodated in the formulation. The crux of the present model lies in the adoption of the periodic boundary conditions in the cross-stream direction imposed on the successive base plates.

For the horizontally-oriented channel, the flow patterns, in particular, in the regions immediately behind the last block, are sensitive to the change of Gr/Re^2. The buoyancy effects have profound influences in determining the thermal fields. The local Nusselt number over the surface of the block is the highest for the first block, and it decreases progressively for the downstream blocks. The temperature field and heat transfer along the surface of the base plate are presented. They reveal the inadequacy of such simplified assumptions as the isothermal or adiabatic base plate conditions.

For the vertically-oriented channel, the impact of the buoyancy effect on the flow and thermal fields is more pronounced. The cooling efficiency, as measured by the reduction of the maximum block temperature, is slightly higher for the vertically-oriented channel. In the case of the vertical channel, the buoyancy effect aids the forced convection; therefore, the heat transfer is augmented. The present results based on the conjugate heat transfer analyses suggest that the adiabatic

or isothermal base plate conditions are not fully compatible with realistic systems.

Acknowledgements—The authors appreciate the detailed and helpful suggestions of the referees. These constructive comments led to substantial improvements in the paper. This work was supported in part by research grants from the Korean Ministry of Science and Technology and from the Advanced Fluids Engineering Research Center of Pohang Institute of Science and Technology, Pohang, Korea.

REFERENCES

1. A. D. Kraus and A. Bar-Cohen, *Thermal Analysis and Control of Electronic Equipment*. Hemisphere, New York (1983).
2. S. Ramadhyani, D. F. Moffatt and F. P. Incropera, Conjugate heat transfer from small isothermal heat sources embedded in a large substrate, *Int. J. Heat Mass Transfer* **28,** 1945–1952 (1985).
3. J. Davalath and Y. Bayazitoglu, Forced convection cooling across rectangular blocks, *J. Heat Transfer* **109,** 321–327 (1987).
4. Y. Jaluria, *Natural Convection*, HMT Vol. 5. Pergamon Press, Oxford (1980).
5. L. Pera and B. Gebhart, Laminar plume interactions, *J. Fluid Mech.* **68**(2), 259–271 (1975).
6. Y. Jaluria, Interaction of natural convection wakes arising from thermal sources on a vertical surface, *ASME National Heat Transfer Conf. on Heat Transfer in Electronic Equipment*, pp. 67–76 (1984).
7. S. Habchi and Y. Acharya, Laminar mixed convection in a partially blocked vertical channel, *Int. J. Heat Mass Transfer* **29,** 1711–1722 (1986).
8. K. J. Kennedy and A. Zebib, Combined free and forced convection between horizontal parallel plates; some case studies, *Int. J. Heat Mass Transfer* **26,** 471–474 (1983).
9. B. H. Kang, Y. Jaluria and S. S. Tewari, Mixed convection air cooling of an isolated rectangular heat sources module on a horizontal plate, *ASME Proc., National Heat Transfer Conf.*, Vol. 2, pp. 59–66 (1988).
10. S. S. Tewari and Y. Jaluria, Mixed convection transport from heat sources mounted on horizontal and vertical surfaces, *ASME Proc., National Heat Transfer Conf.*, Vol. 2, pp. 67–77 (1988).
11. J. R. Maughan and F. P. Incropera, Experiments on mixed convection heat transfer for airflow in a horizontal and inclined channel, *Int. J. Heat Mass Transfer* **30,** 1307–1318 (1987).
12. M. E. Braaten and S. V. Patankar, Analysis of laminar mixed convection in shrouded arrays of heat rectangular blocks, *Int. J. Heat Mass Transfer* **28,** 1699–1709 (1985).
13. S. V. Patankar, C. H. Liu and E. M. Sparrow, Fully developed flow and heat transfer in ducts having streamwise-periodic variations of cross-sectional area, *J. Heat Transfer* **99,** 180–186 (1977).
14. S. V. Patankar and C. Prakash, An analysis of the effect of plate thickness on laminar flow and heat transfer in interrupted plate passages, *Int. J. Heat Mass Transfer* **24,** 1801–1810 (1981).
15. M. Kelkar and S. V. Patankar, Numerical prediction of flow and heat transfer in parallel plate channel with staggered fins, *J. Heat Transfer* **109,** 25–30 (1987).
16. W. Knight and M. E. Crawford, Numerical prediction of turbulent flow and heat transfer in channels with periodically varying cross sectional area, *ASME Proc., National Heat Transfer Conf.*, Vol. 1, pp. 669–676 (1988).
17. Y. M. Chen and Y. Kuo, Interferometric studies on forced convection cooling across rectangular blocks, *3rd Int. Symp. on Transport Phenomena in Thermal Control*, pp. 85–96 (1988).
18. S. V. Patankar, *Numerical Heat Transfer and Fluid Flow*. McGraw-Hill, New York (1980).
19. S. K. Park and K. S. Chang, Pattern of interactive natural convection from two horizontal square cylinders, *Int. Commun. Heat Mass Transfer* **14,** 429–436 (1987).

CONVECTION MIXTE SUR DES BORDURES MULTI-COUCHES AVEC DES CONDITIONS AUX LIMITES PERIODIQUES TRANSVERSALES

Résumé—On analyse les caractéristiques de l'écoulement et du transfert thermique en convection mixte dans un canal avec des blocs rectangulaires attachés à une paroi du canal. On modélise le refroidissement des chips à haute puissance montées sur un système de circuit imprimé. On résout numériquement les équations de Navier–Stokes dans l'hypothèse de Boussinesq. On tient compte de l'épaisseur finie de la paroi et on décrit le caractère conjugué du transfert thermique dans un module. On impose la condition aux limites thermiquement périodique sur les deux plaques successives. On détaille l'écoulement et le champ thermique pour des nombres de Reynolds allant de 100 à 1500, des nombres de Grashof de 0 à 2×10^6, pour deux cas représentatifs : un canal horizontal et un canal vertical. On considère le nombre de Nusselt local le long des surfaces du block, les distributions de la température et de la densité de flux sur la surface de base de la plaque. On décrit le comportement de la température maximale de la chip vis-à-vis de *Re*. On peut affirmer que des hypothèses trop simplificatrices comme surface de paroi isotherme ou adiabatique ne sont pas appropriées pour simuler le refroidissement des équipements électroniques modernes.

MISCHKONVEKTION AN MEHRSCHICHTIGEN PLATTEN MIT PERIODISCHEN RANDBEDINGUNGEN

Zusammenfassung—Es werden Strömung und Wärmeübergang bei Mischkonvektion in einem Kanal mit rechteckigen Blöcken an einer der Wände untersucht. Mit dieser geometrischen Anordnung wird die Kühlung integrierter Schaltkreise (IC) mit hoher Leistungsdichte, die auf einer mehrschichtigen gedruckten Schaltung aufgebracht sind, modelliert. Aus den zugrundeliegenden Navier Stokes Gleichungen ergeben sich unter der Annahme eines Boussinesq-FLuides umfassende numerische Lösungen. Die endliche Dicke der Platte wird vollständig berücksichtigt. Die konjugierten Wärmetransportvorgänge in einem einzelnen Modul werden beschrieben. Um stärker an die Realität heranzukommen, wird die thermisch-periodische Randbedingung zwei aufeinander folgenden Platten aufgeprägt. Für Reynolds-Zahlen im Bereich von 100 bis 1500 und Grashof-Zahlen im Bereich von 0 bis 2×10^6 werden Einzelheiten der Strömungs- und Temperaturfelder für zwei repräsentative Fälle gezeigt, nämlich einen waagerechten und einen senkrechten Kanal. Das Verhalten der örtlichen Nusselt-Zahl entlang der Blockoberfläche wird abgebildet. Die Verteilung von Temperatur- und Wärmestromdichte auf der Oberfläche der Grundplatte wird veranschaulicht. Der Verlauf der maximalen Chiptemperatur über der Reynolds-Zahl wird beschrieben. Aus der vorgestellten Untersuchung der konjugierten Wärmeübertragung folgt, daß die zu stark vereinfachenden Annahmen einer isothermen oder adiabaten Randbedingung an der Wandoberfläche ungeeignet für die Simulation der Kühlung moderner elektronischer Komponenten sind.

СМЕШАННАЯ КОНВЕКЦИЯ ОТ МНОГОСЛОЙНЫХ ПЛАТ С ПЕРИОДИЧЕСКИ ИЗМЕНЯЮЩИМИСЯ ГРАНИЧНЫМИ УСЛОВИЯМИ

Аннотация—Анализируются характеристики течения и теплопереноса при смешанной конвекции в канале с прямоугольными перегородками на одной стенке. Геометрия течения моделирует процесс охлаждения интегральных чипов с высокими мощностями, установленных в системе многослойных печатных плат. Получено большое количество численных решений определяющих уравнений Навье–Стокса в приближении Буссинеска. При учете конечной толщины платы описывается взаимосвязанный характер теплопереноса в единичном модуле. С целью приближения к реальным условиям на две последовательно расположенные пластины налагается периодически изменяющееся тепловое граничное условие. Представлены характеристики полей течения и температур при числе Рейнольдса, изменяющемся от 100 до 1500, и числе Грасгофав в интервале от 0 до 2×10^6 для двух типичных случаев, а именно, с горизонтальной и вертикальной ориентацией канала. Приведены значения локального числа Нуссельта у поверхностей перегородок и распределения температур и скоростей теплопереноса на поверхности опорной пластины. Изображено изменение максимальной температуры чипа в зависимости от значения Re. На основании представленного анализа взаимосвязанного теплопереноса делается вывод, что упрощенные допущения об изотермичности или адиабатичности стенки могут быть не совсем приемлемыми для моделирования охлаждения современных электронных устройств.